Multimode nonlinear analysis of free-electron laser amplifiers in three dimensions

H. P. Freund
Science Applications International Corporation, McLean, Virginia 22102
(Received 7 October 1987)

The nonlinear evolution of a free-electron laser (FEL) amplifier is investigated for a configuration in which an electron beam propagates through an overmoded rectangular waveguide in the presence of a planar wiggler with parabolically tapered pole pieces. The analysis is fully three dimensional and describes the evolution of an arbitrary number of resonant TE and/or TM modes of the rectangular guide as well as the trajectories of an ensemble of electrons. Numerical simulations are conducted for parameters consistent with the 35-GHz amplifier experiment performed by Orzechowski and co-workers [Phys. Rev. Lett. **54**, 889 (1985); **57**, 2172 (1986)], in which the TE_{01}, TE_{21}, and TM_{21} modes were observed. The theory is found to be in good agreement with the experiment. Surprisingly, comparison with a single-mode analysis shows that the enhancement of the efficiency of the TE_{01} mode obtained by means of a tapered wiggler is significantly greater (as well as being in substantial agreement with the experiment) when the TE_{21} and TM_{21} modes are included in the simulation.

I. INTRODUCTION

The free-electron laser (FEL) has been shown to be a high-power radiation source over a broad spectrum extending from microwave[1-13] through optical[14-21] wavelengths. For operation at relatively low beam energies (typically below about 500 keV) and long wavelengths, the device is termed a Ubitron[1] and the interaction occurs in the vicinity of the lowest-order waveguide cutoff. As a consequence, the system can be designed in such a way that the beam is resonant only with the lowest-order waveguide mode, and a single-mode analysis is sufficient to describe many aspects of the interaction. However, at higher energies and shorter wavelengths, the interaction is overmoded in the sense that the electron beam can be resonant with several (perhaps many) modes, and the competition and interaction between the modes has important consequences for the interaction.

The motivation for the present work is to develop a multimode nonlinear theory and simulation code for a Ubitron FEL amplifier which employs a planar wiggler. This general configuration has been extensively studied in the linear regime.[22-27] The present nonlinear analysis is based on previously described single-mode nonlinear analyses of a helical-wiggler–axial-guide-field[28-31] and planar-wiggler[32] configurations. The development of a multimode analysis represents a straightforward generalization of the single-mode theories, and involves the calculation of $\mathbf{J}\cdot\mathbf{E}$ for each mode as well as the integration of electron trajectories in the aggregate field composed of the sum of all the resonant modes. The particular configuration considered in the present work is that of a planar-wiggler geometry in which the electron beam propagates through a rectangular waveguide, although multimode analyses can also be developed for optical Gaussian resonator modes.[33-35] The detailed wiggler model we employ includes the effect of parabolically shaped pole pieces in order to provide for electron focusing in the plane of the bulk wiggler motion,[1,36] and we model the injection of the electron beam into the wiggler by allowing the wiggler amplitude to increase adiabatically from zero to a constant level. In addition, we consider the effect of a tapered wiggler amplitude on efficiency enhancement in overmoded systems. As in the case of the single-mode analysis,[32] the overlap between the electron beam and the transverse-mode structure of either TE or TM modes is included in a self-consistent way, and no arbitrary "filling factor" is necessary. Although the problem of interest is that of an overmoded FEL amplifier which requires a multimode treatment, only single-frequency propagation need be considered. As a result, Maxwell's equations may be averaged over a wave period which results in the elimination of the fast-time-scale phenomena from the formulation.

The organization of the paper is as follows. The general formulation is described in Sec. II, and allows for the inclusion of an arbitrary number of modes of TE and/or TM polarization, subject to the restriction that all are propagating modes at the same frequency. A direct application of the multimode analysis is to the description of a recent experiment by Orzechowski and coworkers,[9,13] in which the TE_{01}, TE_{21}, and TM_{21} modes of a rectangular waveguide were observed. Numerical examples appropriate to this experiment are discussed in Sec. III, and good agreement with the experiment is found. A summary and discussion is given in Sec. IV.

II. GENERAL FORMULATION

The configuration we employ is that of an electron beam propagating through an overmoded rectangular waveguide in the presence of a planar-wiggler field generated by a magnet array with parabolically tapered pole pieces.[1,36] As a result, the wiggler field is assumed to be of the form

$$\mathbf{B}_w(\mathbf{x})=B_w\left\{\cos k_w z\left[\sinh\left[\frac{k_w x}{\sqrt{2}}\right]\sinh\left[\frac{k_w y}{\sqrt{2}}\right]\hat{\mathbf{e}}_x+\cosh\left[\frac{k_w x}{\sqrt{2}}\right]\cosh\left[\frac{k_w y}{\sqrt{2}}\right]\hat{\mathbf{e}}_y\right]\right.$$
$$\left.-\sqrt{2}\cosh\left[\frac{k_w x}{\sqrt{2}}\right]\sinh\left[\frac{k_w y}{\sqrt{2}}\right]\sin(k_w z)\hat{\mathbf{e}}_z\right\}, \tag{1}$$

where B_w denotes the wiggler amplitude and k_w ($\equiv 2\pi/\lambda_w$) is the wiggler wave number. The injection of the beam into the wiggler is modeled by an adiabatic increase in the wiggler amplitude over N_w periods. In addition, since the enhancement of the efficiency by means of a tapered wiggler is also studied, the wiggler amplitude will be tapered downward starting at some point z_0 downstream from the entry region in a linear fashion. For this purpose we choose

$$B_w(z)=\begin{cases}B_w\sin^2(k_w z/4N_w), & 0\le z\le N_w\lambda_w\\ B_w, & N_w\lambda_w<z\le z_0\\ B_w[1+\epsilon_w k_w(z-z_0)], & z>z_0\end{cases} \tag{2}$$

where

$$\varepsilon_w\equiv\frac{1}{k_w}\frac{d}{dz}\ln B_w \tag{3}$$

describes the slope of the taper. Since the fringing fields associated with the tapered wiggler amplitude are neglected, this representation requires the slopes of the taper to be small (i.e., N_w must be large and $|\varepsilon_w|\ll 1$).

The boundary conditions at the waveguide wall may be satisfied by expanding the vector potential in terms of the orthogonal basis functions of the vacuum waveguide. Thus we write the vector potential of the radiation in the form

$$\delta\mathbf{A}(\mathbf{x},t)=\sum_{l,n=0}^{\infty}{}'\,\delta A_{ln}(z)\mathbf{e}_{ln}^{(1)}(x,y)\cos\alpha \tag{4}$$

for the TE modes and

$$\delta\mathbf{A}(\mathbf{x},t)=\sum_{l,n=1}^{\infty}\delta A_{ln}(z)\left[\mathbf{e}_{ln}^{(2)}(x,y)\cos\alpha+\frac{k_{ln}}{k}\sin\left[\frac{l\pi X}{a}\right]\right.$$
$$\left.\times\sin\left[\frac{n\pi Y}{b}\right]\sin\alpha\hat{\mathbf{e}}_z\right] \tag{5}$$

for the TM modes, where, for frequency ω and wave number $k(z)$,

$$\alpha\equiv\int_0^z dz'k(z')-\omega t\ . \tag{6}$$

In addition, $\sum'$ indicates that l and n are not both zero, and

$$\hat{\mathbf{e}}_{l,n}^{(1)}(x,y)\equiv\frac{n\pi}{k_{ln}b}\cos\left[\frac{l\pi X}{a}\right]\sin\left[\frac{n\pi Y}{b}\right]\hat{\mathbf{e}}_x$$
$$-\frac{l\pi}{k_{ln}a}\sin\left[\frac{l\pi X}{a}\right]\cos\left[\frac{n\pi Y}{b}\right]\hat{\mathbf{e}}_y\ , \tag{7}$$

$$\mathbf{e}_{ln}^{(2)}(x,y)\equiv\frac{l\pi}{k_{ln}a}\cos\left[\frac{l\pi X}{a}\right]\sin\left[\frac{n\pi Y}{b}\right]\hat{\mathbf{e}}_x$$
$$+\frac{n\pi}{k_{ln}b}\sin\left[\frac{l\pi X}{a}\right]\cos\left[\frac{n\pi Y}{b}\right]\hat{\mathbf{e}}_y \tag{8}$$

are the polarization vectors. In this representation, the waveguide is assumed to be centered at the origin and bounded by $-a/2\le x\le a/2$ and $-b/2\le y\le b/2$. As a consequence, $X\equiv x+a/2$, $Y\equiv y+b/2$, and

$$k_{ln}\equiv\pi\left[\frac{l^2}{a^2}+\frac{n^2}{b^2}\right]^{1/2} \tag{9}$$

denotes the cutoff wave vector. It is implicitly assumed that both $\delta A_{ln}(z)$ and $k(z)$ vary slowly over a wave period.

The multimode treatment includes an arbitrary number of propagating modes of TE and/or TM polarization. The detailed equations which describe the evolution of the amplitudes and wave numbers of these modes are identical to those derived in the single-mode analysis,[32] and we merely restate the results here. The equations which govern the evolution of the TE_{ln} mode are

$$\frac{d^2}{dz^2}\delta a_{ln}+\left[\frac{\omega^2}{c^2}-k^2-k_{ln}^2\right]\delta a_{ln}=8\frac{\omega_b^2}{c^2}F_{ln}\left\langle\frac{\cos\alpha}{|v_z|}\mathbf{e}_{ln}^{(1)}\cdot\mathbf{v}\right\rangle \tag{10}$$

and

$$2k^{1/2}\frac{d}{dz}(k^{1/2}\delta a_{ln})=-8\frac{\omega_b^2}{c^2}F_{ln}\left\langle\frac{\sin\alpha}{|v_z|}\mathbf{e}_{ln}^{(1)}\cdot\mathbf{v}\right\rangle\ , \tag{11}$$

where $\delta a_{ln}\equiv e\delta A_{ln}/mc^2$, $\omega_b^2\equiv 4\pi n_b e^2/m$ (where n_b is the bulk density of the beam), $\mathbf{v}$ is the instantaneous electron velocity, and $F_{ln}\equiv\frac{1}{2}$ when either $l=0$ or $n=0$, and unity otherwise. For the TM_{ln} mode we obtain a similar result,

$$\frac{d^2}{dz^2}\delta a_{ln}+\left[1+\frac{k_{ln}^2}{k^2}\right]\left[\frac{\omega^2}{c^2}-k^2-k_{ln}^2\right]\delta a_{ln}=8\frac{\omega_b^2}{c^2}\left\langle\frac{\cos\alpha}{|v_z|}\mathbf{e}_{ln}^{(2)}\cdot\mathbf{v}+\frac{v_z}{|v_z|}\frac{k_{ln}}{k}\sin\left[\frac{l\pi X}{a}\right]\sin\left[\frac{n\pi Y}{b}\right]\sin\alpha\right\rangle \tag{12}$$

and

$$2\left[k+\frac{k_{ln}2}{k}\right]^{1/2}\frac{d}{dz}\left[\left[k+\frac{k_{ln}2}{k}\right]^{1/2}\delta a_{ln}\right]=-8\frac{\omega_b^2}{c^2}\left\langle\frac{\sin\alpha}{|v_z|}\mathbf{e}_{ln}^{(2)}\cdot\mathbf{v}-\frac{v_z}{|v_z|}\frac{k_{ln}}{k}\sin\left[\frac{l\pi X}{a}\right]\sin\left[\frac{n\pi Y}{b}\right]\cos\alpha\right\rangle\ , \tag{13}$$

where we note that there is no nontrivial TM-mode solution when $l=0$ and $n=0$.

Equations (10)–(13) are equivalent to a calculation of $\mathbf{J}\cdot\delta\mathbf{E}_{ln}$ for each mode. The averaging operator $\langle(\cdots)\rangle$ is defined over the initial conditions of the beam, and includes the effect of an *initial* momentum spread by means of the distribution function

$$F_0(\mathbf{p}_0)=A\exp[-(p_{z0}-p_0)^2/\Delta p_z^2]\delta(p_0^2-p_{10}^2-p_{z0}^2)H(p_{z0}) , \tag{14}$$

where p_0 and Δp_z describe the initial bulk momentum and momentum spread, $H(x)$ is the Heaviside function, and the normalization constant is

$$A\equiv\left[\pi\int_0^{p_0}dp_{z0}\exp[-(p_{z0}-p_0)^2/\Delta p_z^2]\right]^{-1} . \tag{15}$$

Observe that this distribution is *monoenergetic,* but contains a pitch-angle spread which describes an *axial* energy spread given approximately by

$$\frac{\Delta\gamma_z}{\gamma_0}\simeq 1-\left[1+2(\gamma_0^2-1)\frac{\Delta p_z}{p_0}\right]^{-1/2} , \tag{16}$$

where $\gamma_0\equiv(1+p_0^2/m^2c^2)^{1/2}$. As a result, the averaging operator takes the form

$$\langle(\cdots)\rangle\equiv\frac{A}{2\pi ab}\int_0^{2\pi}d\phi_0\int_0^{p_0}dp_{z0}\beta_{z0}\exp[-(p_{z0}-p_0)^2/\Delta p_z^2]\int_{-\pi}^{\pi}d\psi_0\sigma_{\parallel}(\psi_0)\int_{-a/2}^{a/2}dx_0\int_{-b/2}^{b/2}dy_0\sigma_{\perp}(x_0,y_0)(\cdots) , \tag{17}$$

where $\psi_0\,(\equiv-\omega t_0)$ is the initial ponderomotive phase, $\phi_0\equiv\tan^{-1}(p_{y0}/p_{x0})$, $\beta_{z0}\equiv v_{z0}/c$, and $\sigma_{\parallel}(\psi_0)$ and $\sigma_{\perp}(x_0,y_0)$ describe the initial-beam distributions in phase and in the cross section.

The phase variation of each mode can be analyzed by the addition of an equation to integrate the relative phase:

$$\Phi(z)\equiv\int_0^z dz'[k(z')-k_0] , \tag{18}$$

where $k_0\equiv(\omega^2/c^2-k_{ln}^2)^{1/2}$, is the wave number of the vacuum guide. Since the departure of $k(z)$ from the vacuum wave number describes the effect of the wave-particle interaction, $\Phi(z)$ represents a measure of the dielectric effect of the FEL interaction. Thus we integrate the additional equation

$$\frac{d}{dz}\Phi=k-k_0 , \tag{19}$$

for each TE and TM mode.

Each mode will interact resonantly with the electrons and be coupled through the electron motion in the combined wiggler and bulk radiation fields. Thus in order to complete the formulation, the electron orbit equations must also be specified. Since we describe an amplifier model, we choose to integrate in z, and write the Lorentz force equations in the form

$$v_z\frac{d}{dz}\mathbf{p}=-e\delta\mathbf{E}-\frac{e}{c}\mathbf{v}\times(\mathbf{B}_w+\delta\mathbf{B}) , \tag{20}$$

where $\mathbf{B}_w$ is given by Eq. (1) and the radiation fields are given by

$$\delta\mathbf{E}=-\frac{1}{c}\frac{\partial}{\partial t}\sum_{\text{all modes}}\delta\mathbf{A}_{ln} \tag{21}$$

and

$$\delta\mathbf{B}=\nabla\times\sum_{\text{all modes}}\delta\mathbf{A}_{ln} . \tag{22}$$

Finally the electron coordinates obey the equations

$$v_z\frac{d}{dz}x=v_x , \tag{23}$$

$$v_z\frac{d}{dz}y=v_y , \tag{24}$$

and

$$\frac{d}{dz}\psi=k+k_w-\frac{\omega}{v_z} , \tag{25}$$

which describe the evolution of ponderomotive phase

$$\psi=\psi_0+\int_0^z dz'\left[k+k_w-\frac{\omega}{v_z}\right] . \tag{26}$$

III. NUMERICAL ANALYSIS

The dynamical equations for the particles and fields described in Sec. II are now solved for an overmoded amplifier configuration in which several modes may be in resonance with the beam at a fixed frequency ω. The numerical problem involves the solution of a set of $6N_T+4N_M$ ordinary differential equations (where N_T is the number of particles and N_M is the number of modes) as an initial-value problem. Observe that equations for the amplitude, growth rate, wave number, and phase are integrated for each mode. The integration is accomplished by means of a fourth-order Runge-Kutta-Gill technique, and the particle average described in Eq. (17) is performed by and Nth-order Gaussian quadrature in each of the initial variables. The initial conditions on the fields are chosen to model the injection of an arbitrary power level of each mode, and the initial wave numbers correspond to the vacuum state [i.e., $k(z=0)=k_0$]. Further, the initial value of the relative phase of each mode is zero, and both the wiggler field and growth rate are initially zero. The initial state of the electron beam is chosen to model the injection of a continuous, axisymmetric electron beam with a uniform cross section so that $\sigma_{\parallel}=1$ for $-\pi\le\psi_0\le\pi$ and $\sigma_{\perp}=1$ for $r_0\le R_b$. A more

detailed description of the procedure is to be found in Refs. 22 and 26.

The particular example we consider is that of a 35-GHz amplifier employing an electron beam with an energy of 3.5 MeV, a current of 850 A, and an initial radius of 1.0 cm propagating through a waveguide characterized by $a=9.8$ cm and $b=2.9$ cm. Wave-particle resonance is obtained in the vicinity of 35-GHz for a wiggler field of 3.72-kG amplitude and a 9.8-cm period, and beam injection is accomplished over an entry with a length of five wiggler periods. For this choice of parameters three wave modes are resonant; specifically, the TE_{01}, TE_{21}, and TM_{21} modes. The multimode results described herein will be compared with a previous single-mode treatment. In addition, the parameters correspond with an experiment conducted by Orzechowski and coworkers,[9,13] and a comparison of the simulation with the experiment will be given in Sec. IV.

The detailed evolution of the total wave power as a function of axial position is shown in Fig. 1 for an axial energy spread of $\Delta\gamma_z/\gamma_0=1.5\%$ on the beam and the injection of a signal at $\omega/ck_w=11.3$ (34.6 GHz) composed of the TE_{01} mode at 50 kW, the TE_{21} mode at 500 W, and the TM_{21} mode at 100 W. As shown in the figure, saturation of the total signal occurs at $k_w z=96$ (1.5 m) at a power level of 201 MW for a total efficiency of $\eta\simeq 6.87\%$. It is also evident that although the TE_{01} mode was the overwhelming dominant mode upon injection, it comprises only about 60% of the signal at saturation. The remaining power is composed primarily of the TE_{21} mode (at 37% of the signal) with only a relatively small contribution of the TM_{01} mode. As discussed in Ref. 32, the reason for this is that at this frequency the growth rate of the TE_{21} mode exceeds that of the TE_{01} mode, and compensates for the lower initial power level. Due to the polarization of the TM_{21} mode, the growth rate and efficiency are smaller than for the TE modes, and the TM_{21} mode never accounts for more than about 7 MW. The rapid oscillation shown in the figure has a period of approximately $\lambda_w/2$ and occurs because the evolution of $\mathbf{J}\cdot\mathbf{E}$ for a planar wiggler exhibits both a slow variation corresponding to the ponderomotive phase and a rapid oscillation at $\lambda_w/2$.[32] Observe that the single-mode analysis showed a saturated power of 162 MW for the TE_{01} mode, 126 MW for the TE_{21} mode, and 25 MW for the TM_{21} mode. Thus while the total power of the signal in the multimode analysis somewhat exceeds that shown in the single-mode cases (for the TE modes), the power levels of the individual modes are lower.

The phase variation of each of these modes is shown in Fig. 2 as a function of axial position, where the arrow denotes the point at which the total power saturates. Of these modes, the TE_{01} mode qualitatively behaves in the same way as in the single-mode case. Specifically, the bulk phase at this frequency (apart from the rapid oscillation at $\lambda_w/2$) increases monotonically with axial position through, and beyond, the saturation point. In contrast, the relative phases of both the TE_{21} and TM_{21} modes are decidedly not monotonic and exhibit a decrease with axial position starting at a point somewhat beyond saturation. This is a multimode effect since the relative phases of the TE_{21} and TM_{21} modes also exhibit a monotonic increase with axial position at this frequency in the single-mode analysis. Finally, we observe that the curves of rel-

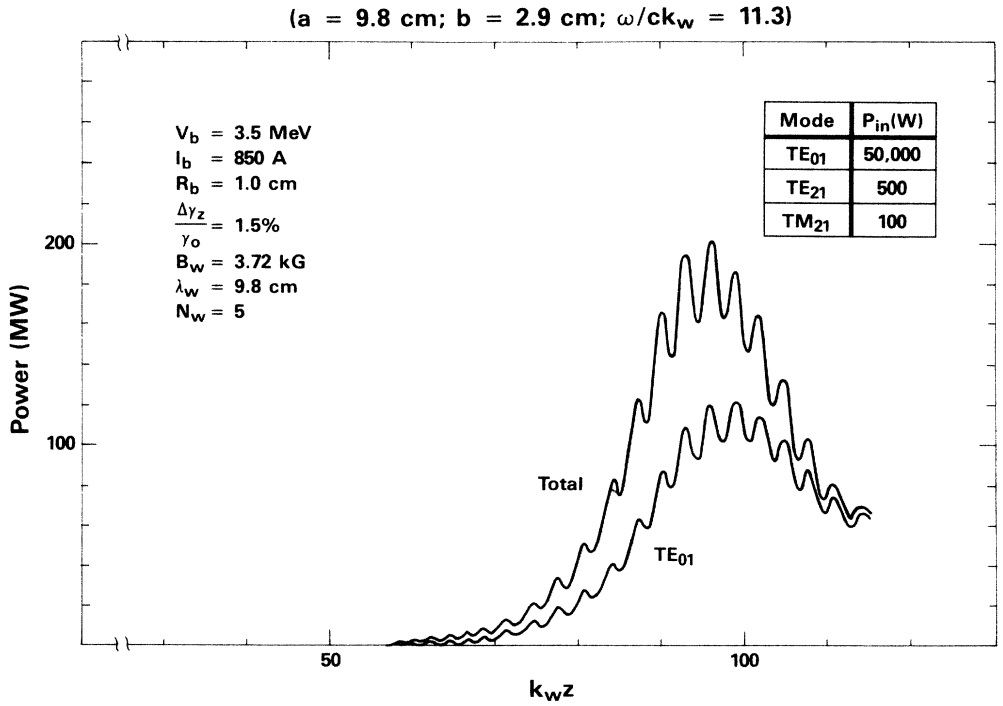

FIG. 1. Evolution of the wave power (both total and TE_{01} model) with axial position.

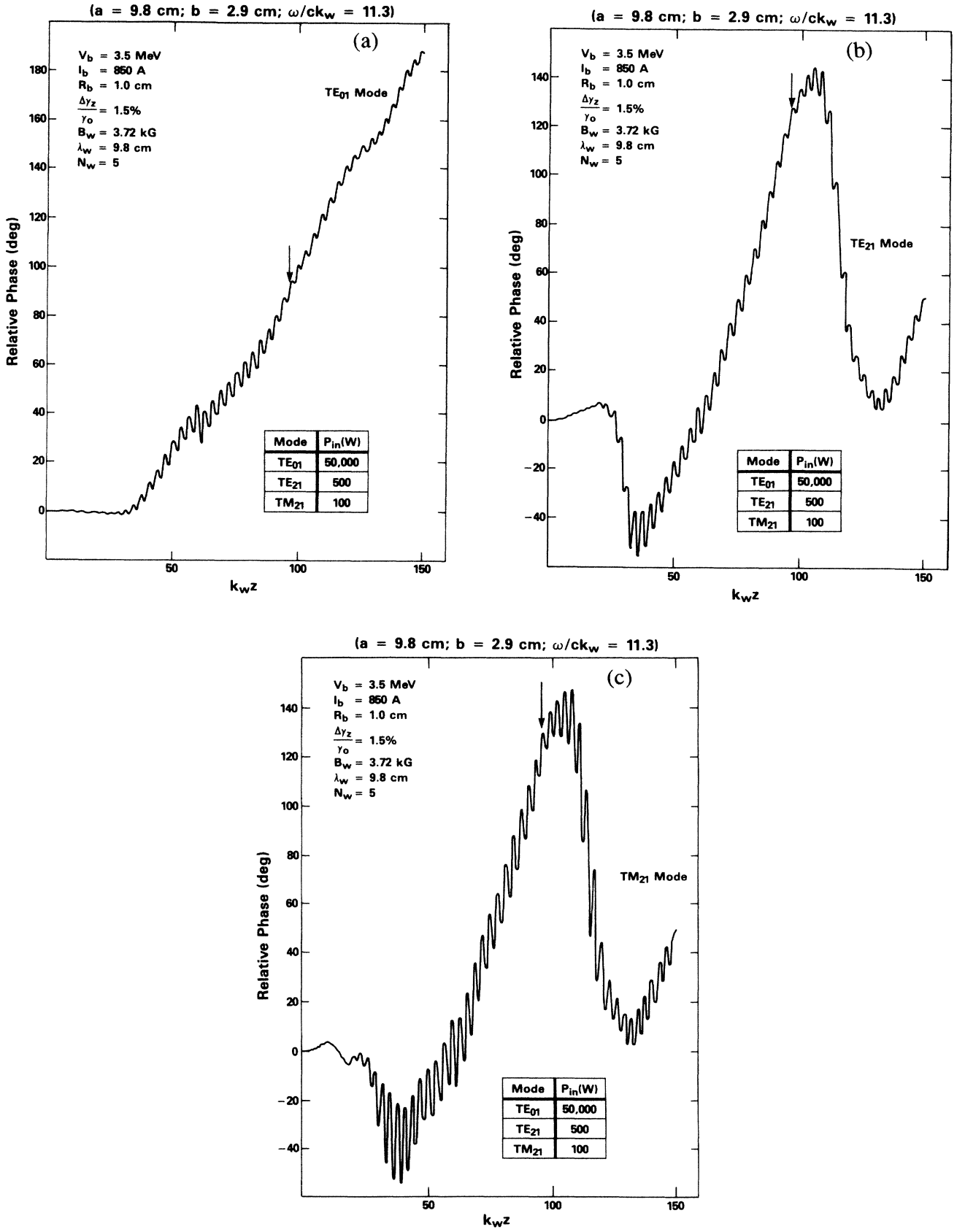

FIG. 2. Plots of the evolution of the relative phase vs axial position for (a) the TE_{01} mode, (b) the TE_{21} mode, and (c) the TM_{21} mode.

ative phase for the TE_{21} and TM_{21} modes are almost identical. The reason for this is that the dispersion curves for the TE_{ln} and TM_{ln} modes are degenerate in a rectangular waveguide.

The effect of an initial momentum spread on the saturation efficiency of the total signal and the TE_{01} and TE_{21} mode components is shown in Fig. 3. The TM_{21} mode is excluded from the figure because it composes such a small fraction of the signal. As shown in the figure, the saturation efficiency is *relatively* insensitive to the axial energy spread over the range $\Delta\gamma_z/\gamma_0 \lesssim 2.5\%$, and decreases from $\eta \simeq 8.6\%$ at $\Delta\gamma_z \simeq 0$ to $\eta \simeq 5.9\%$ at $\Delta\gamma_z/\gamma_0 \simeq 2.5\%$. The reason for this is that the coupling coefficient (and, hence, the growth rate) depends upon the product of the wiggler amplitude and period. Since this product is large for the present choice of parameters, the growth rate is large and the interaction can accept a relatively large axial energy spread without suffering a severe degradation.

The saturation efficiency is known to scale as the cube root of the beam current at the frequency of peak growth from the idealized one-dimensional theory of the high-gain Compton (i.e., the strong-pump) regime, and this type of scaling law was also found from the three-dimensional single-mode simulation of this configuration. The scaling of the total power as a function of beam current for the multimode analysis is shown in Fig. 4 for $\Delta\gamma_z=0$ and $\Delta\gamma_z/\gamma_0=1\%$, and the efficiency is found to scale approximately as $\eta \sim I_b^{1/3}$.

Turning to the question of the enhancement of the efficiency by means of a tapered wiggler, we plot the evolution of the power with axial position in Fig. 5 for parameters corresponding to those shown in Fig. 1. The optimal start-taper point for this case is $k_w z_0 = 86$, and we choose a slope of $\epsilon_w = -0.007$, which was also studied for the single-mode analysis. The central conclusion to be drawn from the figure is that it is possible to selectively enhance the TE_{01} mode. The uniform wiggler interac-

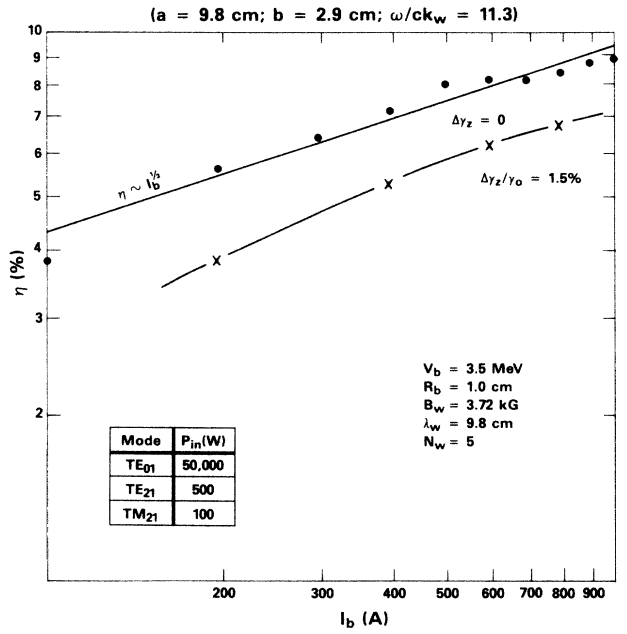

FIG. 4. Graph showing the scaling of the efficiency of the total signal with beam current for $\Delta\gamma_z/\gamma_0=0$ and 1%.

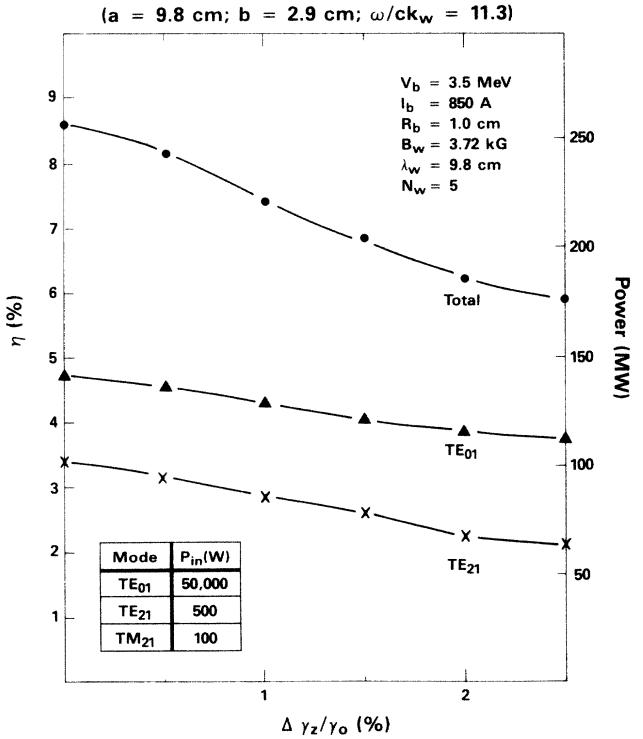

FIG. 3. Variations of the saturation efficiencies of the total signal and the TE modes vs axial energy spread.

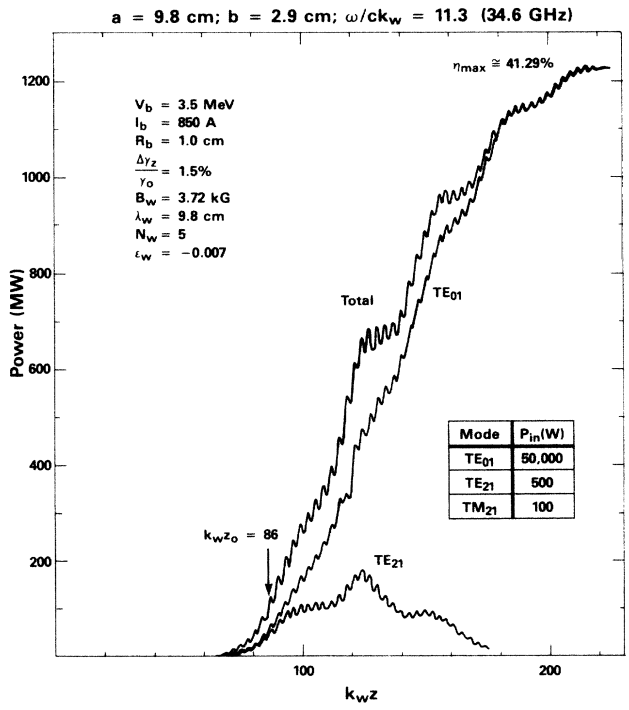

FIG. 5. Plot showing the evolution of the total signal and the TE modes for a tapered wiggler interaction characterized by $\epsilon_w = -0.007$ and $k_w z_0 = 86$.

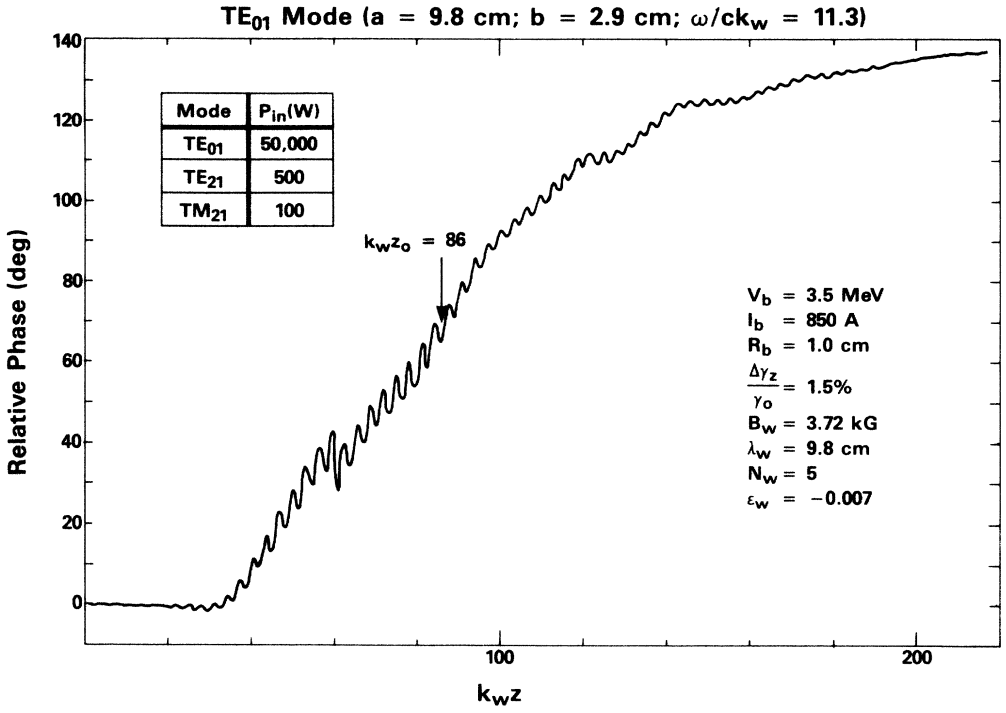

FIG. 6. Graph of the evolution of the relative phase of the TE_{01} mode during the course of the tapered wiggler interaction.

tion for this example yields a total efficiency of 6.8%, of which the TE_{01} mode comprises only 60% of the signal. By contrast, careful choice of both the start-taper point and the slope of the taper shows that the efficiency can be enhanced to $\eta_{max} \simeq 41.29\%$ (if the wiggler field is tapered to zero) with 99% of the power in the TE_{01} mode. Both the TE_{21} and TM_{21} (not shown in the figure) modes ultimately decay to extremely low intensities. One surprising result of the present multimode analysis is that the maximum efficiency to be obtained by tapered wiggler fields is enhanced relative to the single-mode analysis. By comparison, the single-mode analysis for these parameters yields a maximum efficiency of $\eta_{max} \simeq 34\%$, which is substantially lower than the 41.29% found in the multimode simulation. The phase variation of the TE_{01} mode for this example is shown in Fig. 6, and exhibits the same qualitative variation as in the single-mode analysis. Another characteristic of the tapered wiggler interaction observed in the single-mode treatment is that the overall efficiency appears to be relatively insensitive to the axial energy spread. As shown in Fig. 7, in which we plot the maximum obtainable efficiency versus $\Delta\gamma_z/\gamma_0$, this is also found to be the case in the multimode analysis. As shown in the figure, the maximum efficiency decreases from 43.6% at $\gamma_z = 0$ to as much as 39.4% at $\Delta\gamma_z/\gamma_0 = 2\%$. This is a much lower proportional sensitivity to the axial energy spread than is illustrated in Fig. 3 for the uniform wiggler case.

Finally, we address the question of the sensitivity of the tapered wiggler interaction to fluctuations in the bulk energy of the beam. The reason for concern with this is-

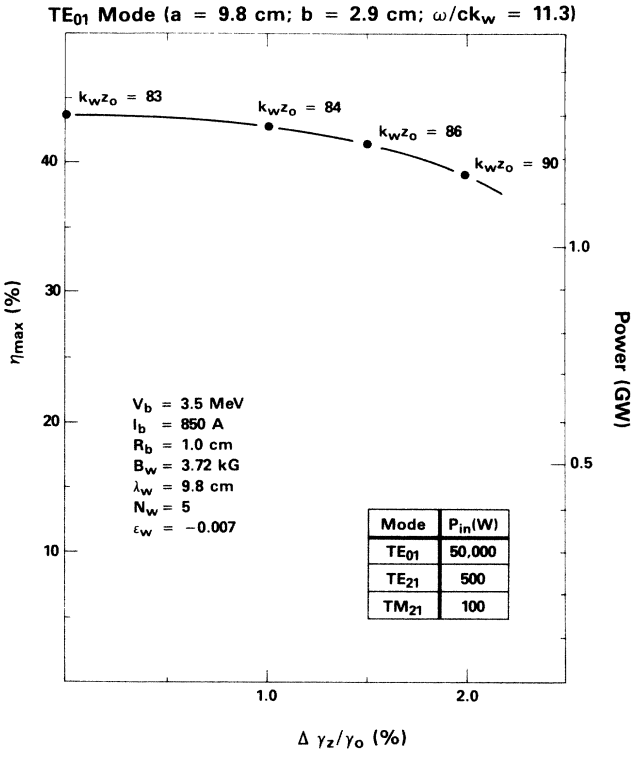

FIG. 7. Illustration of the effect of an axial energy spread on the tapered wiggler interaction. Observe that each point corresponds to the optimal start-taper point of the associated $\Delta\gamma_z$.

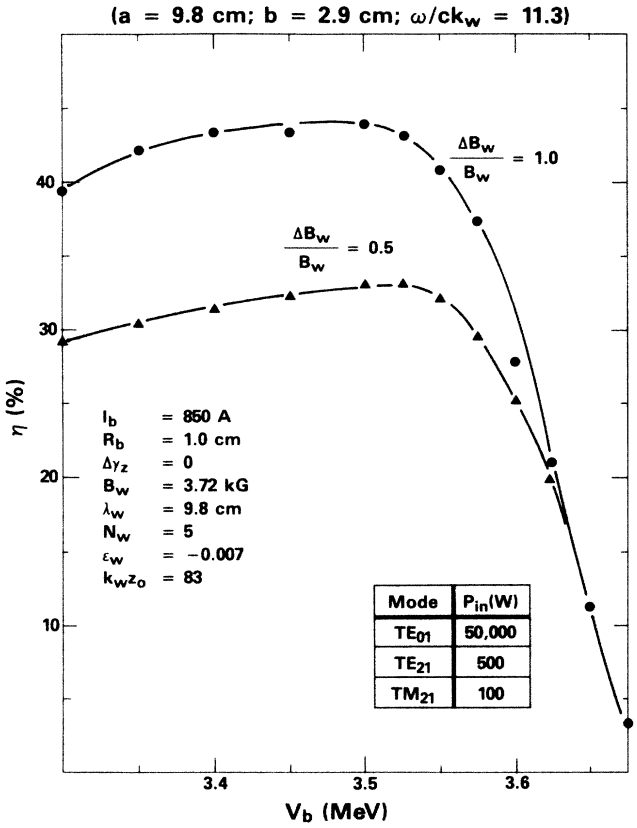

FIG. 8. Variation in the efficiency of the tapered wiggler interaction with fluctuations in the bulk energy of the beam.

sue is that the tapered wiggler interaction is known to be sensitive to the start-taper point. In particular, the taper should begin at a point shortly prior to saturation (for the untapered wiggler), corresponding to the trapping of the bulk of the beam in the ponderomotive potential. Changes or fluctuations in the beam energy at a fixed frequency are equivalent to the variation of the frequency at fixed energy, and result in shifts in the growth rate and saturation point. For this reason it might be expected that the tapered wiggler interaction is sensitive to fluctuations in the bulk energy of the beam. In order to address this question, the variation in the efficiency has been studied as a function of beam energy, and the results are shown in Fig. 8. For convenience, this figure has been generated for the limiting case of zero axial energy spread for which the optimal start-taper point is $k_w z_0 = 83$ at a beam energy of 3.5 MeV. Hence, choosing $\epsilon_w = -0.007$ and the aforementioned start-taper point, Fig. 8 describes the variation in the efficiency with beam energy when (1) the wiggler is tapered to zero ($\Delta B_w/B_w = 1$) and (2) when the wiggler is tapered to half its ambient level ($\Delta B_w/B_w = 0.5$). As shown in the figure, there is a sharp decline in the efficiency above, approximately, 3.55 MeV. In contrast, there is a more gradual decrease in the efficiency for energies down to 3.3 MeV, below which the resonant interaction at $\omega/ck_w = 11.3$ is lost. As a result, the tapered wiggler interaction will tolerate a bulk energy fluctuation of the order of 8.6% without severe degradation in performance for these parameters.

IV. SUMMARY AND DISCUSSION

In this paper a multimode analysis and simulation of FEL amplifiers in three dimensions has been given for a configuration in which a relativistic electron beam propagates through an overmoded rectangular waveguide in the presence of a planar wiggler generated by means of an array of magnets with tapered pole pieces. The multimode analysis is accomplished by expansion of the radiation field in terms of the vacuum waveguide modes, and an arbitrary number of propagating TE and/or TM modes is included in the analysis. Although multiple modes are included in the analysis, the problem of interest is that of an amplifier and single-frequency propagation. As a result, the field equations are averaged over a wave period in order to eliminate the fast-time-scale phenomena. However, no average of the orbit equations was performed, and the electron dynamics were treated by means of the fully three-dimensional Lorentz force equations. As a result, the effects of the adiabatic injection process, bulk wiggler motion, Betatron oscillations, velocity shear, beam focusing due to the wiggler gradients, and phase trapping of the beam in the ponderomotive potential formed by the beating of the wiggler and radiation fields are all included in a self-consistent manner.

The numerical example describes a 35-GHz amplifier which employs a 3.5-MeV–850-A electron beam with a 1.0-cm initial radius propagating through a rectangular waveguide with dimensions $a = 9.8$ cm and $b = 2.9$ cm in the presence of a wiggler field with a 3.72-kG amplitude and 9.8 cm period. Three distinct wave modes are found to be resonant; specifically, the TE_{01}, TE_{21}, and TM_{21} modes. The simulation is carried out under the assumption that the injected signal consists primarily of the TE_{01} mode at a 50 kW power level, the TE_{21} mode at 500 W, and the TM_{21} mode at 100 W. Results indicate that although the TE_{21} mode was at a relatively low initial power level, it comprises upwards of 37% of the saturated signal. The coupling between the beam and the TM_{21} mode was weaker than for the TE modes, and never accounted for more than a few percent of the total signal. Comparison with a previous single-mode analysis[32] indicates that the efficiency of the total signal is somewhat higher than that found for single modes in the case of a uniform wiggler. A more dramatic difference between the multimode and single-mode treatments is found for a tapered wiggler interaction. In this case, it is found that the selective enhancement of the TE_{01} mode is possible and, indeed, has been experimentally observed.[13] However, the power levels to be obtained in the TE_{01} mode through the multimode tapered wiggler interaction were found to be *substantially* higher than found in the single-mode simulation. This constitutes an important question for future study.

The configuration and parameters described in this paper nominally correspond to the experiment performed by Orzechowski and co-workers.[9,13] The principal

differences between the analytical configuration and the experiment are that in the experiment (1) the beam was injected into the wiggler through an entry taper region one-wiggler-period long and (2) a quadrupole field was used to provide additional electron focusing instead of parabolically tapered pole pieces. Since the fringing fields associated with the wiggler field in the entry taper region are not included in the analytical model, it would be invalid to apply the analysis for $N_w=1$. However, the choice of $N_w=5$ is made as a compromise and gives good agreement with experiment, subject to the additional assumption of an axial energy spread of $\Delta\gamma_z/\gamma_0=1.5\%$. This is within an upper bound of 2% on the axial energy spread established by means of an electron spectrometer measurement.[37] The experimental measurement for a uniform wiggler interaction resulted in a saturated power level of 180 MW over a length of 1.3 m. As shown by Fig. 1, the simulation gives a *peak power* of 204 MW, which, if we average over the fast $\lambda_w/2$ oscillation, is reduced to 185 MW. Given the experimental uncertainties in high-power measurements, the latter figure is more relevant for comparison and is in substantial agreement with the experiment. The saturation length found from simulation (that is, the length of the uniform wiggler region plus one wiggler period to account for the entry taper region) is 1.1 m, which is also in good agreement with the experiment. Note that rapid oscillation in the power and relative phase at a period of $\lambda_w/2$ is likely to introduce a 10–20% uncertainty in the measurement of

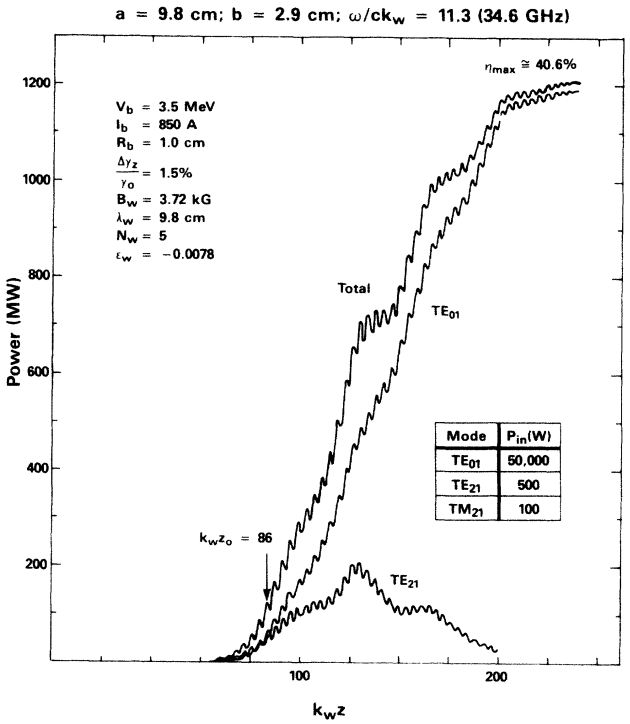

FIG. 9. Plot of the evolution of the total signal and the TE modes for a tapered wiggler characterized by $\epsilon_w=-0.0078$ and $k_wz_0=86$.

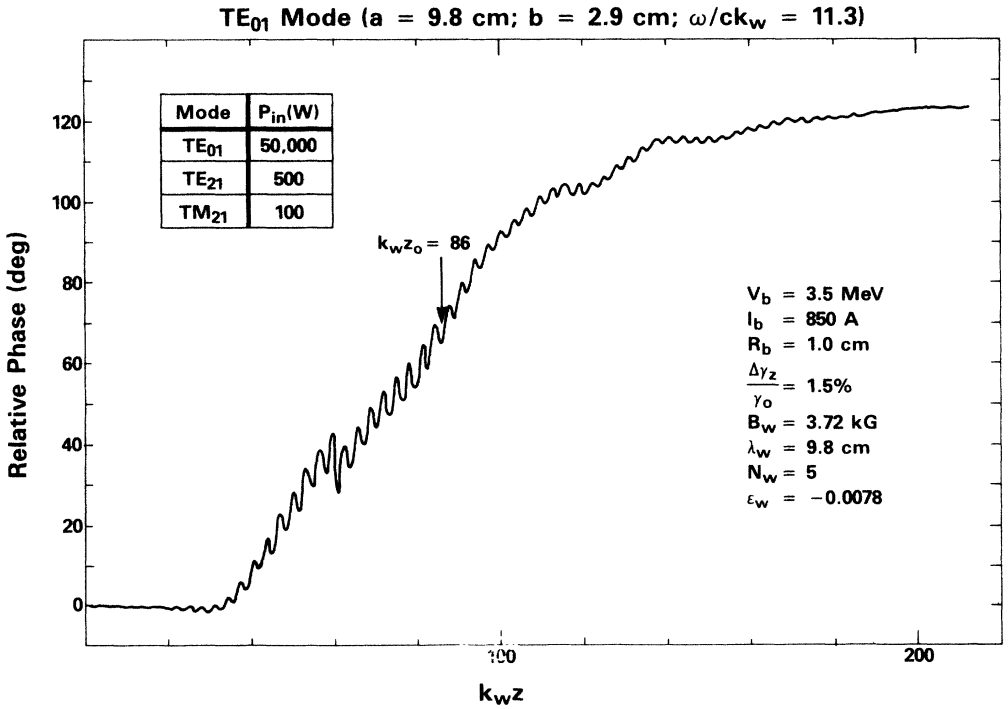

FIG. 10. Graph of the evolution of the relative phase for a tapered wiggler interaction characterized by $\epsilon_w=-0.0078$ and $k_wz_0=86$.

these quantities. A comparison can also be made with the tapered wiggler experiment[13] in which the wiggler field was decreased by 55% ($\Delta B_w/B_w=0.55$) over a length of 1.1 m (i.e., $\epsilon_w=-0.0078$) and the efficiency was found to increase to 34% for a total power of 1 GW. The evolution of the total signal power, and that of the TE modes, is shown in Fig. 9 for parameters consistent with the tapered wiggler experiment (the optimal start-taper point found in simulation was $k_w z_0=86$). As shown in the figure, the maximum efficiency obtained by tapering the wiggler field to zero is approximately 40.6%, of which more than 95% of the power is contained in the TE_{01} mode. However, over a length of only 1.1 m beyond the start-taper point (i.e., $k_w z-k_w z_0=70.5$) the efficiency is 34%, of which approximately 90% of the power is in the TE_{01} mode. The evolution of the relative phase for this case is shown in Fig. 10, in which the relative phase saturates at a value in the neighborhood of 120° downstream from the start-taper point. This is in good agreement with reported measurements of the evolution of the relative phase in the tapered wiggler experiment.[38] Thus within the uncertainties imposed by the choices of N_w and $\Delta\gamma_z$, the nonlinear analysis is found to be in good agreement with the experimental measurements for both uniform and tapered wiggler interactions.

ACKNOWLEDGMENTS

This research was supported by the U. S. Office of Naval Research and the U. S. Office of Naval Technology. The author would like to thank Dr. A. K. Ganguly, Dr. R. K. Parker, and Dr. R. H. Jackson for helpful discussions.

[1]R. M. Phillips, IRE Trans. Electron. Devices 7, 231 (1960).
[2]V. L. Granatstein, S. P. Schlesinger, M. Herndon, R. K. Parker, and J. A. Pasour, Appl. Phys. Lett. **30**, 384 (1977).
[3]D. B. McDermott, T. C. Marshall, S. P. Schlesinger, R. K. Parker, and V. L. Granatstein, Phys. Rev. Lett. **41**, 1368 (1978).
[4]R. K. Parker, R. H. Jackson, S. H. Gold, H. P. Freund, V. L. Granatstein, P. C. Efthimion, M. Herndon, and A. K. Kinkead, Phys. Rev. Lett. **48**, 238 (1982).
[5]J. Fajans, G. Bekefi, Y. Z. Yin, and B. Lax, Phys. Rev. Lett. **53**, 246 (1984).
[6]J. A. Pasour, R. F. Lucey, and C. W. Roberson, Proc. Soc. Photo-Opt. Instrum. Eng. **453**, 328 (1984).
[7]J. A. Pasour, R. F. Lucey, and C. A. Kapetanakos, Phys. Rev. Lett. **53**, 1728 (1984).
[8]S. H. Gold, D. L. Hardesty, A. K. Kinkead, L. R. Barnett, and V. L. Granatstein, Phys. Rev. Lett. **52**, 1218 (1984).
[9]T. J. Orzechowski, B. Anderson, W. M. Fawley, D. Prosnitz, E. T. Scharlemann, S. Yarema, D. Hopkins, A. C. Paul, A. M. Sessler, and J. Wurtele, Phys. Rev. Lett. **54**, 889 (1985).
[10]J. Fajans, G. Bekefi, Y. Z. Yin, and B. Lax, Phys. Fluids **28**, 1995 (1985).
[11]J. Masud, T. C. Marshall, S. P. Schlesinger, and F. G. Yee, Phys. Rev. Lett. **56**, 1567 (1986).
[12]J. Fajans, J. Wurtele, G. Bekefi, D. S. Knowles, and K. Xu, Phys. Rev. Lett. **57**, 579 (1986).
[13]T. J. Orzechowski, B. Anderson, J. C. Clark, W. M. Fawley, A. C. Paul, D. Prosnitz, E. T. Scharlemann, S. Yarema, D. B. Hopkins, A. M. Sessler, and J. Wurtele, Phys. Rev. Lett. **57**, 2172 (1986).
[14]L. R. Elias, W. M. Fairbanks, J. M. J. Madey, H. A. Schwettman, and T. I. Smith, Phys. Rev. Lett. **36**, 717 (1976).
[15]D. A. G. Deacon, L. R. Elias, J. M. J. Madey, G. J. Ramian, H. A. Schwettman, and T. I. Smith, Phys. Rev. Lett. **38**, 892 (1977).
[16]R. W. Warren, B. E. Newnam, J. G. Winston, W. E. Stein, L. M. Young, and C. A. Brau, IEEE J. Quantum Electron. **QE-19**, 391 (1983).
[17]M. Billandon, P. Ellaume, J. M. Ortega, C. Bazin, M. Bergher, M. Velghe, Y. Petroff, D. A. G. Deacon, K. E. Robinson, and J. M. J. Madey, Phys. Rev. Lett. **51**, 1652 (1983).
[18]J. M. Slater, J. L. Adamski, D. C. Quimby, T. L. Churchill, L. Y. Nelson, and R. E. Center, IEEE J. Quantum Electron. **QE-19**, 374 (1983).
[19]J. A. Edighoffer, G. R. Neil, C. E. Hess, T. I. Smith, S. W. Fornaca, and H. A. Schwettman, Phys. Rev. Lett. **52**, 344 (1984).
[20]B. E. Newnam, R. W. Warren, R. L. Sheffield, W. E. Stein, M. T. Lynch, J. S. Faser, J. C. Goldstein, J. E. Solid, T. A. Swann, J. M. Watson, and C. A. Brau, IEEE J. Quantum Electron. **QE-21**, 867 (1985).
[21]C. R. Pidgeon, S. D. Smith, W. J. Firth, D. A. Jorosynski, D. M. Tratt, J. S. Mackay, M. F. Kimmitt, J. M. Reid, M. G. Kelliher, M. W. Poole, G. Saxon, R. P. Walker, W. A. Gillespie, and P. F. Martin, IEEE J. Quantum Electron. **QE-21**, 1083 (1985).
[22]Y. Z. Yin and G. Bekefi, J. Appl. Phys. **55**, 33 (1983).
[23]T. Shiozawa and H. Nakano, IEEE J. Quantum. Electron. **QE-21**, 931 (1985).
[24]R. C. Davidson and J. Wurtele, IEEE Trans. Plasma Sci. **PS-13**, 464 (1985).
[25]E. Jerby and A. Gover, Nucl. Instrum. Method A **250**, 192 (1986).
[26]R. C. Davidson, Phys. Fluids **29**, 267 (1986).
[27]B. W. J. McNeil and W. J. Firth, Nucl. Instrum. Meth. A **259**, 240 (1987).
[28]A. K. Ganguly and H. P. Freund, Phys. Rev. A **32**, 2275 (1985).
[29]H. P. Freund and A. K. Ganguly, Phys. Rev. A **33**, 1060 (1986).
[30]H. P. Freund and A. K. Ganguly, Phys. Rev. A **34**, 1242 (1986).
[31]H. P. Freund and A. K. Ganguly, IEEE J. Quantum Electron. **QE-23**, 1657, (1987).
[32]H. P. Freund, H. Bluem, and C.-L. Chang, Phys. Rev. A **36**, 2182 (1987).
[33]C. M. Tang and P. Sprangle, IEEE J. Quantum Electron. **QE-21**, 970 (1985).
[34]P. Sprangle, A. Ting, and C. M. Tang, Phys. Rev. Lett. **59**, 202 (!987).
[35]P. Sprangle, A. Ting, and C. M. Tang, Phys. Rev. A **36**, 2773 (1987).
[36]E. T. Scharlemann, J. Appl. Phys. **58**, 2154 (1985).
[37]T. J. Orzechowski (private communication).
[38]T. J. Orzechowski, E. T. Scharlemann, and D. B. Hopkins, Phys. Rev. A **35**, 2184 (1987).